Characterization of Microstructure and Texture across N155 Superalloy Weldment Joint with Austenitic Filler Metal

Morteza Shamanian, Amirkeyvan Rahimi, and Jerzy A. Szpunar

Thin sheets of N155 superalloy were welded by AMS 5832 filler metal using gas tungsten arc welding (GTAW). The purpose of this study is to investigate the characterization of microstructure and texture across the weldment using electron backscatter diffraction (EBSD) technique. The results indicated that N155 superalloy with the crystal lattice (FCC) experienced annealing process before the welding, which made a lot of coherent twins be created in the base metal due to low stacking fault energy (SFE). Moreover, the coherent twins were created mainly in the heat-affected zone by the presence of cumulative stresses of the molten pool solidification shrinkage. Having the same crystal lattice (FCC), the base metal and the weld metal resulted in the formation of epitaxial grains with the preferred growth direction in the weld metal.

1. Introduction

N155 superalloy has excellent resistance in high-temperature corrosive environments (Ref 1-3). Multimet N155 is a nickel-chromium-cobalt alloy with additions of molybdenum and tungsten used typically in parts requiring high strength up to 1350 °F and oxidation resistance up to 1800 °F (Ref 1). N155 superalloy sheets with a variety of alloying elements experienced hot deformation, and then they were heat treated at 1176 °C prior to being quenched in water (annealing process), so this is a solid solution and has sufficient flexibility to provide for fusion welding (Ref 1, 2). After the full recrystallization during hot deformation, a suitable annealing treatment is necessary to improve the microstructures, and to reduce the large residual stress and microcracks. However, due to the unavoidable grain growth during annealing, the final properties of the superalloy can be changed (Ref 4, 5). Twinning is said to have three main sources: mechanical deformation, annealing and transformation (Ref 6). Annealing twinning often occurs in FCC metals, especially in alloys with low stacking fault energy (SFE) (Ref 7). Iron element is not expected to twin unless its SFE is reduced by solid solution (Ref 8) such as N155 superalloy. Chen et al. (Ref 9) and Jin et al. (Ref 10) presented the development of annealing twins during recrystallization and grain growth in pure nickel alloys, and noticed that the grain boundaries movement and the establishment of cube texture could increase the production of annealing twins.

In this study, thin sheets of N155 superalloy were welded using the pulse current that can affect the microstructure of the joint, hence affecting the mechanical properties of the joint. Zhang et al. (Ref 11) showed that using a pulsed current system in the TIG welding process makes the grain orientations be dispersed and grain size smaller in the weld metal of nickel-based superalloy. N155 superalloy is used in numerous aircraft applications including tail cones and tail pipes, exhaust manifolds, combustion chambers, afterburners, turbine blades and buckets; therefore, welding this sensitive alloy with suitable filler metal is an important part of the manufacturing process. There is only limited published literature reported on the welding of N155 superalloy with pulse current mode, let alone EBSD examination of weldment joint. According to the low thickness of N155 superalloy sheet (0.6 mm), it was so difficult to set TIG welding parameters to weld this alloy with a butt joint design by GTAW welder. Moreover, pulsed current gas tungsten arc welding (PC-GTAW) is more economical compared to high-density welding techniques and does not have the problems like vacuum generation and reflection issues. The aim of this study is to investigate the important characterizations of microstructure, which have an important role in determining and explaining the mechanical and corrosion properties such as annealing twins in the base metal (BM) and the heat-affected zone (HAZ), epitaxial growth in the weld metal (WM), grain orientations and distribution of boundaries across similar N155 superalloy weldment joints by austenitic filler metal (AMS 5832) using the EBSD technique. It should be noted that dendritic structures are only noticeable in optical microscopic images of the weld metal and it is difficult to detect grain boundaries in these images; therefore, the EBSD technique is necessary to determine the important characterization of the weld metal microstructure. Moreover, mechanical properties such as microhardness and tensile strength of the joint were investigated by the microstructure results.

Morteza Shamanian and **Amirkeyvan Rahimi**, Department of Materials Engineering, Isfahan University of Technology, Isfahan 8415683111, Iran; and **Jerzy A. Szpunar**, Department of Mechanical Engineering, University of Saskatchewan, Saskatoon, SK S7N 5A9, Canada. Contact e-mail: amirkeyvan.rahimi@ma.iut.ac.ir.

2. Experimental

Thin sheets of N155 alloy with a thickness of 0.6 mm were welded by AMS 5832 filler metal and by using pulsed current gas tungsten arc welding (PC-GTAW). The chemical compositions of both of them are given in Table 1, and details of the welding process are given in Table 2.

The microstructures were examined by Hitachi SU6600 scanning electron microscopy (SEM) equipped with electron backscatter diffraction (EBSD). The diamond polished samples were subsequently polished with 50-nm colloidal silica slurry for 6 h using VibroMet 2 Vibratory polisher (Buehler). To obtain orientation maps, an accelerating voltage of 20 kV, a working distance of 15 mm and a step size of 50 nm were used; in addition, ATEX software was used to obtain EBSD data visualization. According to Fig. 1 in which WD, FD and ND are welding direction, filling direction and normal direction, respectively, ND is parallel to the rolling direction of the base metal.

To examine the microhardness, Vickers method was used with a 100-gf load at intervals of 500 μm. The specimens of the tensile test were prepared according to the ASTM E8 standard; the tensile test was carried out with a crosshead velocity of 1 mm/min at ambient temperature. It should be noted that three numbers of samples are tested to check the data reproducibility.

3. Results and Discussion

3.1 Microstructure and Texture of the Base Metal (BM)

The base metal with low stacking fault energy (SFE) was exposed to annealing process and recrystallization prior to welding. Low SFE metals such as copper, austenitic superalloys or steel contain a high amount of annealing twins (Ref 12). The "coherent twin" is a $<111>$ symmetrical tilt boundary, and the "incoherent twin" is a $<112>$ symmetrical tilt boundary (Fig. 2b). Annealing twinning is created for two reasons: (1) to redirect grain boundaries so as to simplify dislocation absorption and movement during recrystallization (Ref 13), (2) to reduce the entire surface energy when the energy of the boundaries between neighbors of a grain and its twin would be less than that of those between the neighbors and the grain itself (Ref 14). The coherent twins have a significant effect on the microstructure in terms of dislocations slip. It has been accepted that dislocation movement through a $\Sigma 3$ is never a direct transmission; therefore, the twins are effective barriers to slip (Ref 15, 16).

In heavily rolled sheets of metals with the crystal lattice (FCC) and medium-to-high SFE, recrystallization usually leads to an increase in the cube texture with a {100} plane parallel to the rolling plane and a $<100>$ direction along the rolling direction (Ref 17). The lower the SFE makes, the more cube-twin orientations are formed in the recrystallization texture (Ref 17). According to inverse pole figure (IPF) of the BM (Fig. 2c), compression of lines with greater texture intensity in the direction $<001>$ has remained from cube texture with a {100} plane parallel to the rolling plane and a $<100>$ direction along the rolling direction. Moreover, it has medium texture intensity in the direction $<111>$ due to cube-twin orientations in the recrystallization texture (Fig. 2c).

When the metals with medium and low SFE experience the recrystallization, the orientations, which are specified by angles in the range (25°-45°) around axes mostly grouped such as $<122>$, $<012>$, $<112>$ and $<111>$ directions (Ref 18), can be created. It should be noted that these can be the axes grouped around the normals of all four {111} planes (i.e., undergoing twinning in recrystallized grains) (Ref 17). In sheets of FCC metals or alloys of low SFE, the cube texture does not extend during recrystallization. Instead, a texture appears with a main component {236} $<385>$, which is near {113} $<211>$ (Ref 18). Based on the obtained ODFs (Fig. 3), the main components include strong recrystallized brass, $BR = (236) <385>$ and Y-fiber along with Taylor or Dillamore, $D = (4\ 4\ 11) <11\ 11\ 8>$ and weak RG, rotated Goss $= (011) <110$, and other components $(001) <1\ -2\ 0>$, $(111) <1\ -2\ 1>$, $(1\ -1\ 0) <111>$ and $(111) <-1\ -1\ 2>$; and these components are usually found in the modified structure of recrystallization (Ref 17, 19).

3.2 Microstructure and Texture of the Heat-Affected Zone (HAZ)

The heat-affected zone can be divided into two regions based on their distances from the fusion line. The coarse grains structure was formed next to the fusion line due to the larger amount of the weld heat that reaches this region; and the fine grains structure can be seen near the base metal due to the smaller amount of the weld heat that reaches this region, which was less affected by the weld thermal cycle and where the grain growth was less (Fig. 2b).The weld thermal cycle in the heat-affected zone (HAZ) close to the fusion line makes intense microstructural changes in the base metal microstructure (Ref 20, 21). It is believed that twinning occurs either to relieve local stress or to adopt local strain (Ref 22).

Poorhaydari et al. (Ref 23) figured out that the weld effect, especially thermal stress, is an important reason for twinning in the HAZ of low carbon steels. They noticed that the weld thermal stresses/distortions and possibly hydrogen pickup could improve twinning. Hwang and Bernstein (Ref 8) figured out that soluble hydrogen decreases the interatomic energy in iron, resulting in easier separation of the dislocation core and, therefore, helping twin nucleation and growth. Twins can be made due to the internal pressure from the formation of molecular hydrogen in defects.

Table 1 Compositions of the base metal and the filler metal (wt.%)

wt.%	C	Si	Mn	Cr	Co	Ni	Mo	W	Nb	Al	Ti	Fe
N 155 (base metal)	0.12	1	1.5	21.5	20	21	3	2.5	1	…	…	Bal.
AMS 5832 (filler metal)	0.08	0.35	0.35	19	1	52.5	3.1	…	5.1	0.5	0.9	Bal.

Table 2 Welding parameters used in the current work

| Parameter	Value
Shielding/purging gas	99.999% pure argon
Shielding gas flow rate	12 L min^{-1}
Purging gas flow rate	15 L min^{-1}
Filler rod diameter	1.6 mm
Welding electrode	AWS A5.12 EWTH-2 (98% W + 2% ThO$_2$)
Electrode diameter	1.6 mm
Polarity	Direct current electrode negative (DCEN)
Voltage	7.8 V
Frequency	120 Hz
Welding speed	4 cm min^{-1}
I_{av} (pulse current) $= \frac{I_p * t_p + I_b * t_b}{t_p + t_b}$	15 A
I_p (peak current) $= 20$ A and I_b (base current) $= 10$ A, t_p (peak current duration) and t_b (base current duration)	
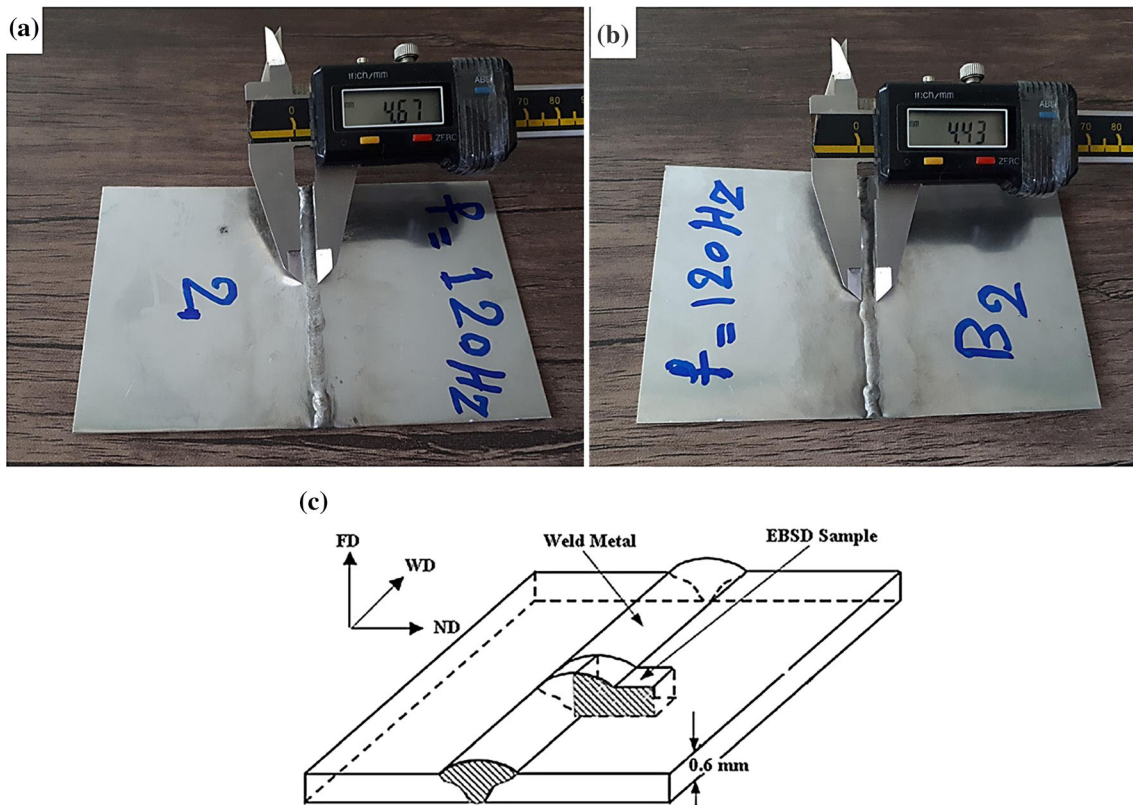
Fig. 1 (a) Front of the welded sample, (b) back of the welded sample, (c) sketch map of the EBSD specimen preparation

N155 superalloy has a low thermal conductivity (12 w/m.k(, which makes the HAZ grains experience high temperature for a long time, so it makes the grain growth and twins formation increase in the region next to the fusion line. The EBSD map of the heat-affected zone (Fig. 2b) shows blue twins. The intensity of coherent twin formation is very high in the HAZ; therefore, it makes the highest texture intensity in the direction of <111> (Fig. 2c).

According to Fig. 4, the intensities of components such as RG and D decreased; however, components BR and (1 −1 0) <111> and TWGC: First-generation Cube-twin = (122) <212> are reinforced by twining, thus increasing the intensity texture that is in the direction of <111>.

3.3 Microstructure and Texture of the Weld Metal (WM)

According to Fig. 2(a), all regions include a single austenite phase with the face-centered cubic lattice (FCC), marked in red, and indicate that the base metal and the weld metal have the same crystal lattice (FCC) and result in the formation of columnar dendrites with the preferred or easy growth orientation <100> along the maximum thermal gradient arising in the WM (Ref 24, 25). During molten pool, solidification grains tend to grow in the orientation perpendicular to pool boundary because this is the orientation of the maximum temperature gradient and results in maximum heat extraction. However, columnar dendrites or cells inside each grain tend to grow in the preferred or easy growth orientation which is <100> for both
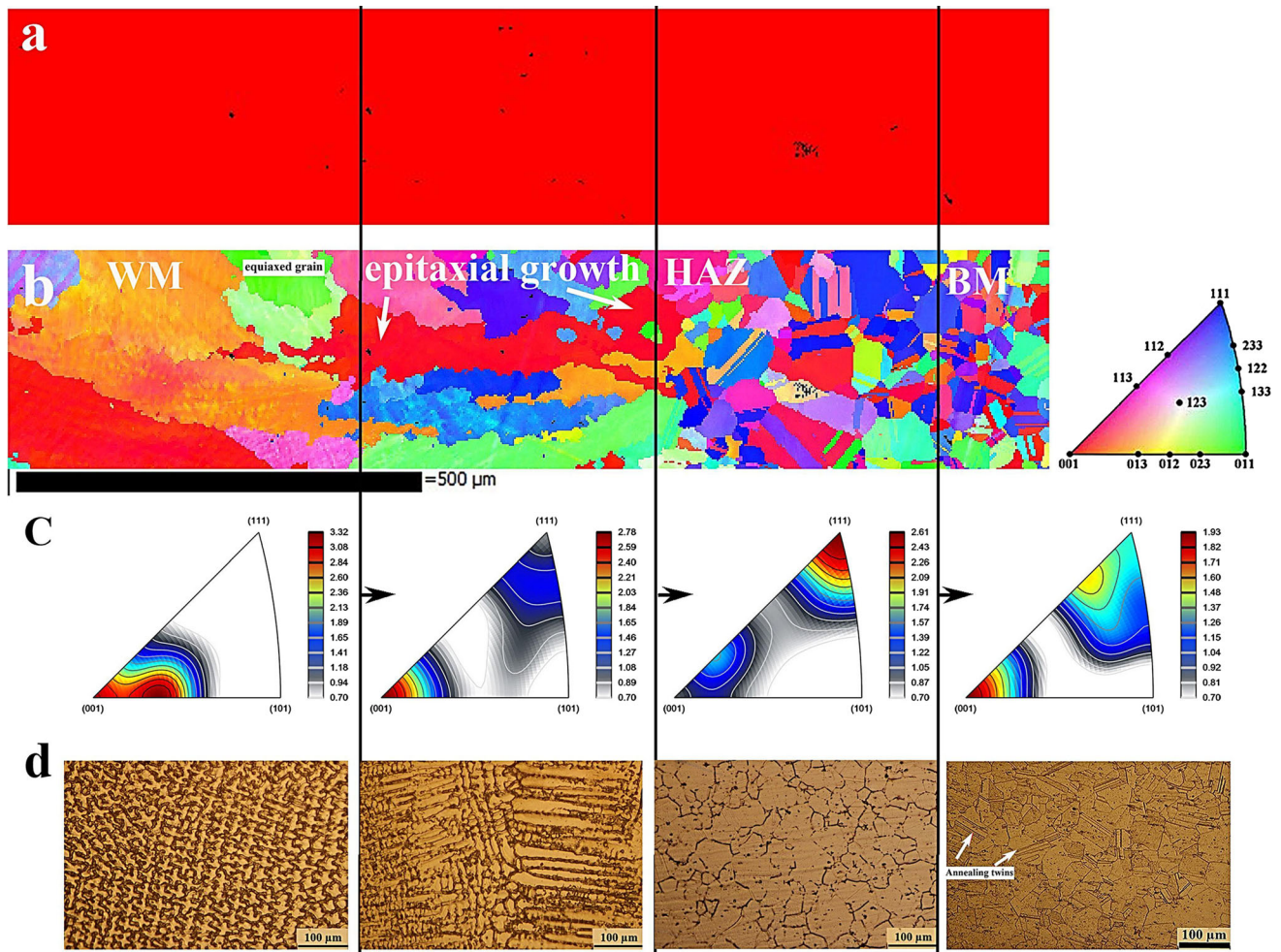
Fig. 2 EBSD maps across the weldment: (a) phase color map, (b) ND IPF map of austenite, (c) triangle of ND inverse pole figure of austenite, (d) the optical micrograph across the welded joint (Color figure online)

FCC and BCC materials (Ref 24). Basak et al. (Ref 26) showed that the epitaxial growth is heterogeneous nucleation, whose nucleus is nucleated from the liquid phase contacted by a solid substrate.

According to Fig. 2(b), in the junction between BM and WM, it can be seen that coarse and long epitaxial grain (red color) grew in the easy growth direction <001>, which contains columnar dendrites, where the highest temperature gradients and G/R ratios (G: temperature gradient, R: growth rate) are high (Ref 27). The extension of the epitaxial [001] directed dendrites adjoining to the BM can be observed (Fig. 2b). The fastest growth orientation for an FCC crystal is the <001> orientation, and hence grain growth is expected to be along <001> crystallographic directions (Ref 28, 29).

Away from the fusion line, an orange grain is seen close to the middle of the WM whose orientation is <013> and where the grain structure is dominated by a different mechanism known as competitive growth (Fig. 2b). The highest texture intensity is also <013>, which can indicate the deviation of grain orientation from the preferred growth orientation <001>

(Fig. 2c). Pollock and Murphy (Ref 30) studied the single crystal solidification in high-refractory nickel-base alloys at different cooling rates. They observed a sharp columnar to equiaxed transition (CET) when thermal gradients were high. For GTAW, welding would be expected to have a sharp CET because of the greater G, and thus a faster (G/R) ratio and higher cooling rate (G.R).

The formation of equiaxed grains is steadfast with the lower G/R ratio expected to grow in the middle of the WM (Ref 31, 32). Thus, the directed columnar dendrites structure next to the BM and randomly directed equiaxed structure in the middle of the WM can be explained by different G/R ratios experienced by fusion welds at these positions. According to Fig. 2(d), the fine dendrites, which are inside equiaxed grains in the center of the WM, are seen.

Based on careful analysis of the WM, some grains are seen in two states as pale and bold color together similar to the pale and bold blue or green that indicate the residual and cumulative stresses due to the weld metal solidification; thus, it affected the colors of grains which are not as the uniform color.
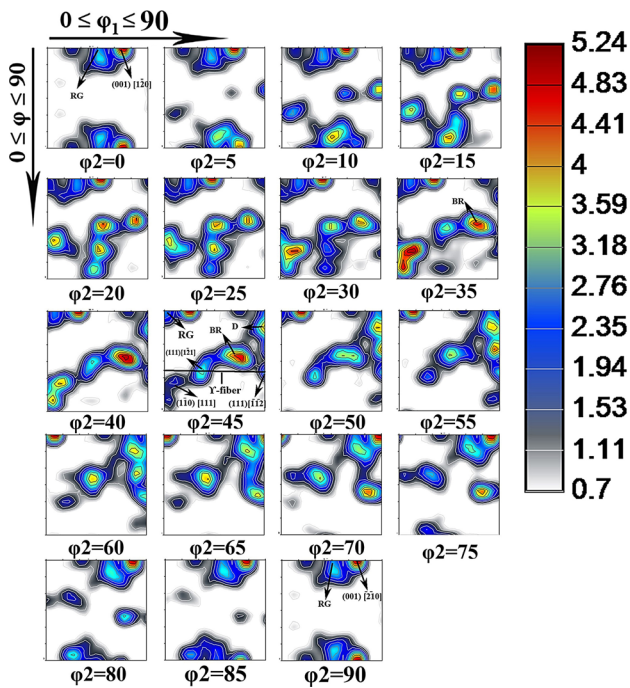
Fig. 3 Constant $\varphi 2$ sections of the orientation distribution function in Euler space in multiples of random density (MRD) for N155 base metal (BM)
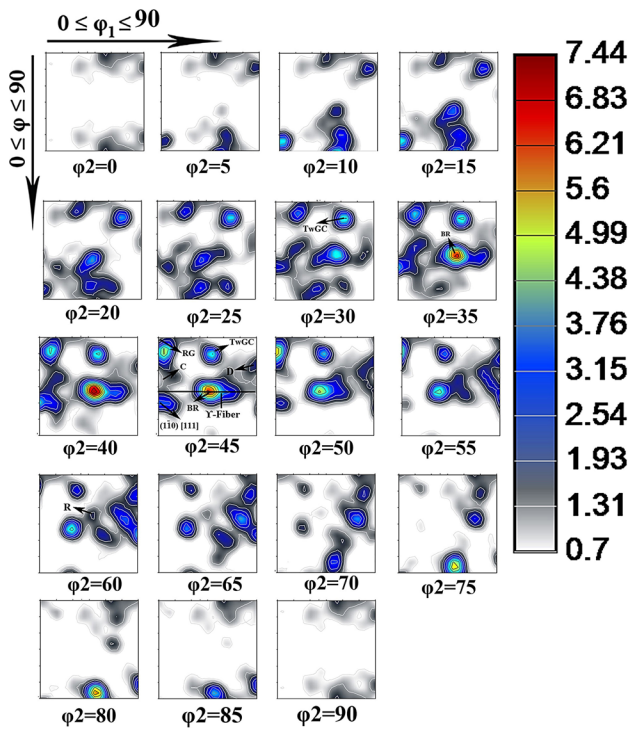

Fig. 4 Constant $\varphi 2$ sections of the orientation distribution function in Euler space in multiples of random density (MRD) for the heat-affected zone (HAZ)

3.4 Grain Boundary Character Distribution

According to the coincident site lattice (CSL) misorientation angle between adjoining grains, boundaries are classified into two categories: (1) The misorientation angle with $2° < \theta < 15°$ is referred to as low-angle grain boundaries (LAGBs or $\Sigma 1$ boundaries), (2) The misorientation angle with $\theta \geq 15°$ is reported as high-angle boundaries (HAGBs). For HAGBs, the grain boundaries with a low CSL value ($1 < \Sigma \leq 29$) are reported as "specific" grain boundaries, whereas others are known as random HAGBs (Ref 33). The specific high-angle boundaries are the relatively coherent interfaces, which have excellent atomic fit and contain few crystalline defects, i.e., low Σ values, are known to have low grain boundary energy compared to random high-angle grain boundaries (Ref 34).

A high concentration of annealing twins ($\Sigma 3^n$; $n = 1, 2, 3$) can modify the fatigue resistance (Ref 35) and hot corrosion resistance of nickel-based superalloys (Ref 36). The generation of $\Sigma 9$ and $\Sigma 27$ boundaries is ascribed to the multiple twinning. According to Fig. 5(a) and (b), in the base metal, it can be found that a lot of annealing twin boundaries with special characters, especially $\Sigma 3$, are characterized by 60° rotation around $<111>$ axis (Fig. 6 and 7), but the fractions of $\Sigma 9$ and $\Sigma 27$ boundaries were extremely limited compared to that of $\Sigma 3$ boundaries. Moreover, coherent annealing twin boundaries with $\Sigma 3$ are the interesting features in polycrystalline superalloys due to their lowest grain boundary energies among low CSL boundaries (Ref 37). In addition, formation of coherent twins can stabilize the HAZ and increase the density of grain boundaries with high angles (HABs) (Ref 38). Thus, according to Fig. 8, there are 99.27% of high-angle boundaries (HABs) with misorientation angles larger than 15° in the HAZ. High fraction of HABs with low Σ values can be seen in this area (Fig. 7). Thus, if a crack is formed, it cannot be easily spread through HABs with low Σ values.

According to Fig. 5(b), high-angle boundaries (HABs) with specific Σ and low energies are found in the epitaxial boundaries and near the interface associated with the base metal, which indicates excellent geometric matching in the boundaries. On the other hand, as we approach the center of welds (equiaxed grains), the density and length of the CSL boundaries are reduced, which indicates an increase in the randomized boundaries with high angles.

Figure 5(c) (KANM across the weldment) shows the increase in density of low-angle or subgrain boundaries (LABs) with misorientation angles of smaller than 5° in the weld metal because this zone has the highest residual stress among other zones due to freezing of the molten pool.

3.5 Mechanical Properties

According to Fig. 9, the microhardness value increases from the interface (WM and HAZ) to the center line of the WM, which is mostly due to the change in the freezing mode from coarse epitaxial grains that contain columnar dendrites to fine equiaxed grains that contain equiaxed dendrites (Fig. 2b, d) associated with increasing microhardness.
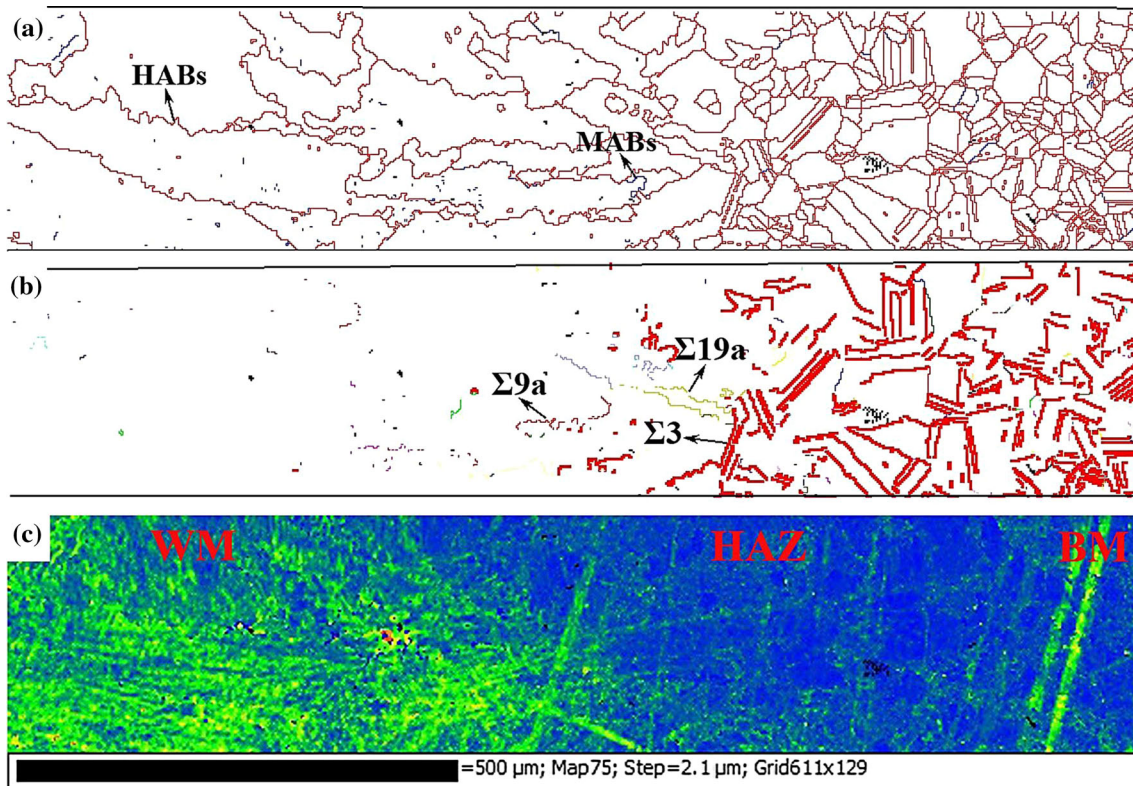
Fig. 5 EBSD results: (a) grain boundaries, (b) CSL boundaries, (c) KANM
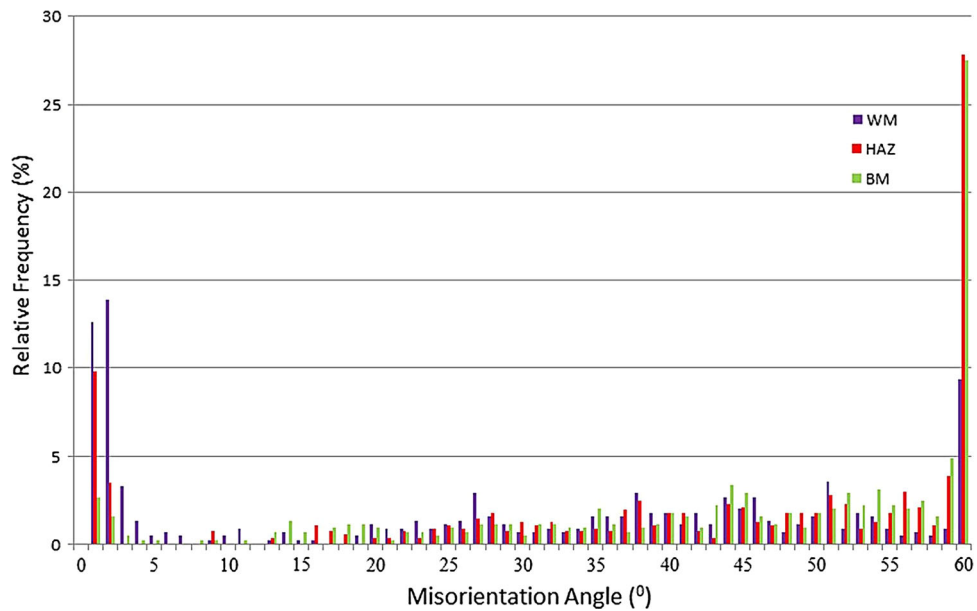

Fig. 6 Distribution of misorientation angle histograms between neighbor grains

The welded sample of the tensile test was made transversely from the weldment, which contains all of the base metal, heat affected and fusion zones. The welded sample was broken from the heat-affected zone with the acceptable tensile strength (746 MPa) (Fig. 10, Table 3). As previously mentioned, the heat-affected zone has coarse grains structure next to the fusion
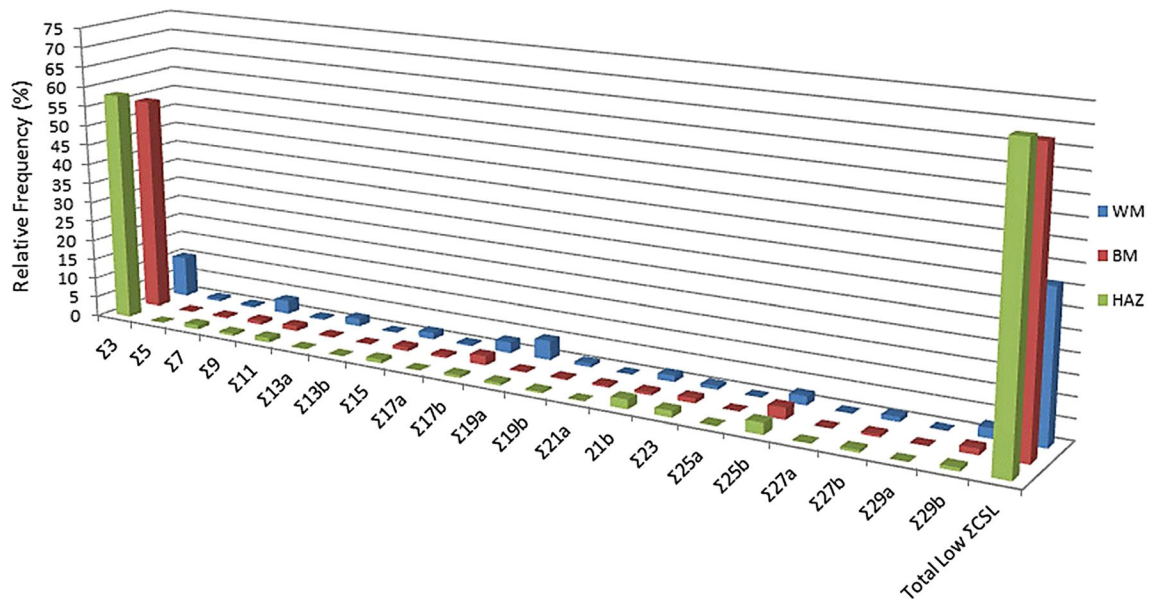
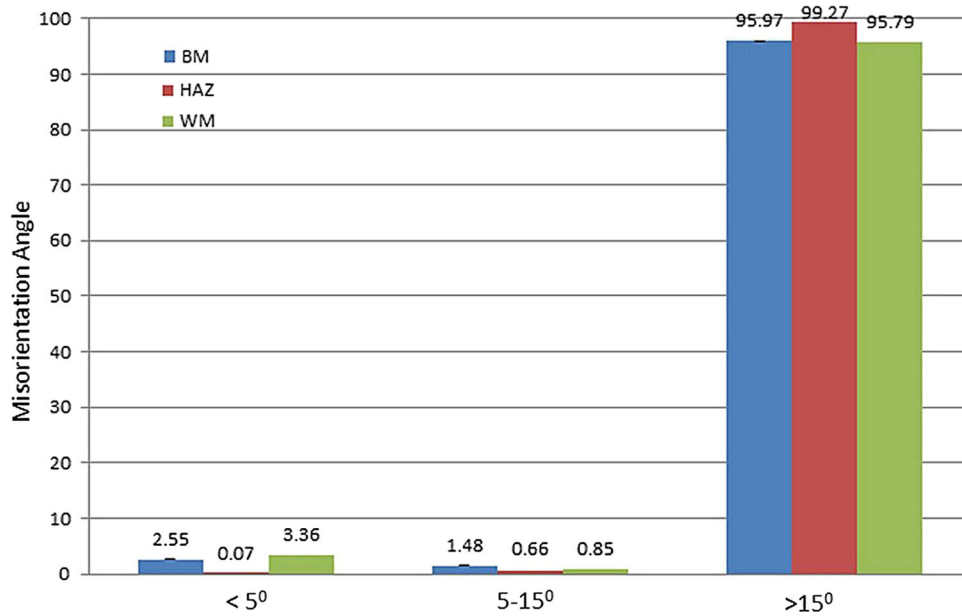**Fig. 7** Distribution of CSL boundaries across the weldment

Fig. 8 Distribution of misorientation angles

line due to the larger amount of the weld heat that reaches this area (Fig. 2b), which makes the HAZ weak in the tensile test. Figure 11(a) shows a soft fracture with a high elongation (40%) in the N155 base metal (BM) sample, and fine and dense dimples with average size (9 μm) can also be seen. In addition, the fracture surface of the welded sample is soft fracture, and coarse dimples can be found (17 μm) with a low elongation (22%) (Fig. 11b, Table 3).

4. Conclusion

The most important results of this study are as follows:

- N155 superalloy with the crystal lattice (FCC) experienced annealing process before the welding, which made a lot of coherent twins be created in the BM due to low SFE.
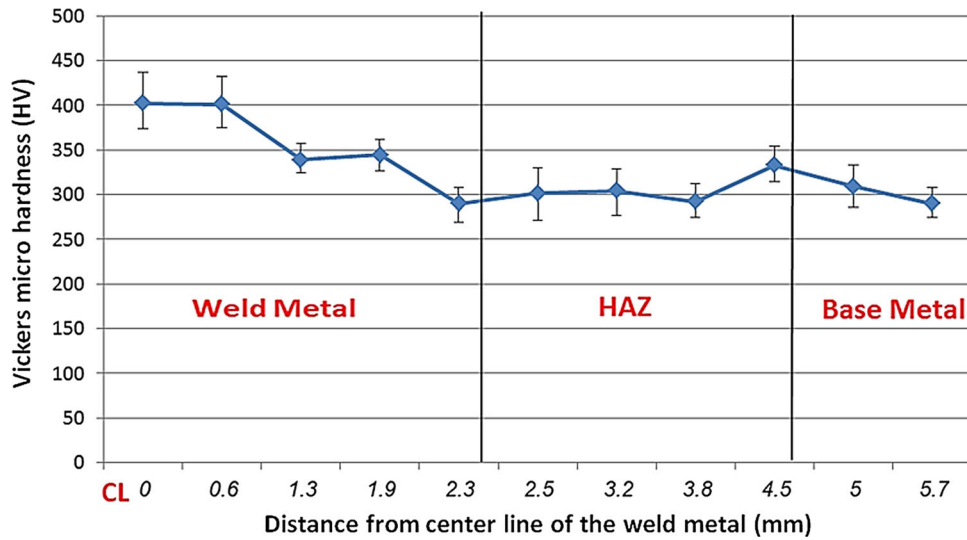
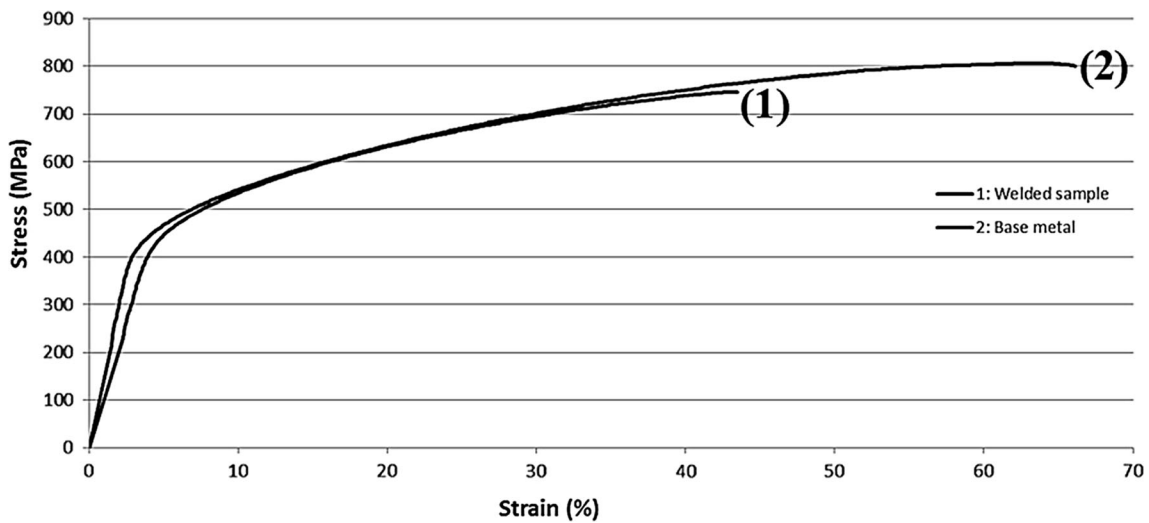**Fig. 9** Microhardness profile of the welded specimen

Fig. 10 Stress–strain diagram of the tensile test

Table 3 Mechanical properties of the specimens

% EL	Ultimate tensile strength, MPa	Yield tensile strength, MPa	Sample
22 ± 0.3	746 ± 8	407 ± 3	WS
40 ± 0.2	806 ± 4	415 ± 5	BM

- Based on analysis of the HAZ, it can be found that formation of coherent twins was caused mainly by the presence of the cumulative stresses of the molten pool solidification shrinkage.
- The base metal and the weld metal with the same crystal lattice (FCC) resulted in the formation of epitaxial grains with the preferred growth direction <001> in the WM.

- The welded sample was broken from the HAZ with the acceptable tensile strength (746 MPa) due to the larger amount of the weld heat that reaches this area, which makes the HAZ weak in the tensile test.
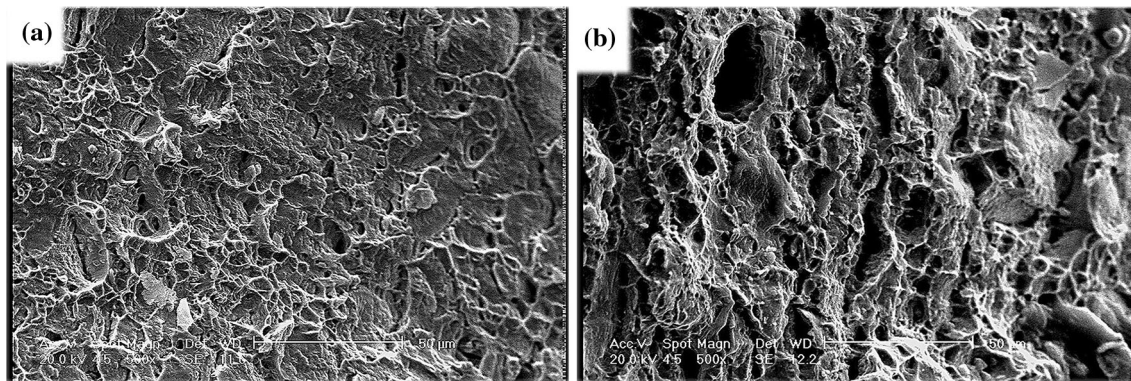
Fig. 11 SEM image of the fracture surface of (a) the BM specimen, (b) the welded specimen

References

1. M.J. Donachie Jr., Relationship of Properties to Microstructure in Superalloys. American Society for Metals. Superalloys Source Book, 1984, p 102–111
2. M. Durand-Charre, *The Microstructure of Superalloys*, CRC Press, Boca Raton, 1998
3. K. Flores and C. Yablinsky, Nickel-Based Superalloys for Advanced Turbine Engines, 2006
4. H.R. Ashtiani and P. Rezaei Karami, Prediction of the Microstructural Variations of Coldeworked Pure Aluminum during Annealing Process, *Model. Numer. Simul. Mater. Sci.*, 2015, **5**, p 1–14
5. C.M. Sellars and J.A. Whiteman, Recrystallization and Grain Growth in Hot Rolling, *Met. Sci.*, 1979, **13**, p 187–194
6. V.K. Heikkinen, Transformation Twins in V-Bearing Mild Steels, *Scand. J. Metall.*, 1974, **3**, p 41–45
7. G.E. Dieter, *Mechanical Metallurgy*, McGraw-Hill Book Company, Maidenhead, 1988
8. C. Hwang and I.M. Bernstein, Hydrogen Induced Slip and Twinning in Iron Alloys, *Scr. Metall.*, 1982, **16**, p 85–90
9. X.P. Chen, L.F. Li, H.F. Sun, L.X. Wang, and Q. Liu, Studies on the Evolution of Annealing Twins during Recrystallization and Grain Growth in Highly Rolled Pure Nickel, *Mater. Sci. Eng. A*, 2015, **622**, p 108–113
10. Y. Jin, B. Lin, M. Bernacki, G.S. Rohrer, A.D. Rollett, and N. Bozzolo, Annealing Twin Development during Recrystallization and Grain Growth in Pure Nickel, *Mater. Sci. Eng. A*, 2014, **597**, p 295–303
11. X.H. Zhang, J.Q. Chen, and K. Zhang, Study on Grain Refinement of Nickel-Based Filler Metal 52 M Microstructure by Pulse TIG Welding, in *2nd International Conference on Mechatronics Engineering and Information Technology (ICMEIT 2017)*, Atlantis Press, 2017
12. V. Randle, Mechanism of Twinning-Induced Grain Boundary Engineering in Low Stacking Fault Energy Materials, *Acta Mater.*, 1999, **47**(15-16), p 4187–4196
13. G. Gindraux and W. Form, New Concepts of Annealing-Twin Formation in Face Centred Cubic Metals, *J. Inst. Metals*, 1973, **101**, p 85–93
14. R.L. Fullman and J.C. Fisher, Formation of Annealing Twins During Grain Growth, *J. Appl. Phys.*, 1951, **22**(11), p 1350–1355
15. B.J. Pestman et al., Interaction Between Lattice Dislocations and Grain Boundaries in FCC and Ordered Compounds: A Computer Simulation, *Philos. Mag. A*, 1991, **64**(4), p 951–969
16. S. Poulat, B. Decamps, and L. Priester, Weak-Beam Transmission Electron Microscopy Study of Dislocation Accommodation Processes in Nickel Σ = 3 Grain Boundaries, *Philos. Mag. A*, 1998, **77**(6), p 1381–1397
17. J. Jensen, Encyclopedia of Materials: Science and Technology, 2001, p 318–322
18. M. Miszczyk, Microstructure and Texture Evolution during Annealing of Plane Strain Compressed Al and Al-1% Mn Alloy Single Crystals, *Arch. Metall. Mater.*, 2011, **56**(4), p 933–938
19. C.W. Sinclair, F. Robaut, L. Maniguet, J.D. Mithieux, J.H. Schmitt, and Y. Brechet, Recrystallization and Texture in a Ferritic Stainless Steel: An EBSD Study, *Adv. Eng. Mater.*, 2003, **5**, p 570–574
20. K.E. Easterling, *Introduction to the Physical Metallurgy of Welding*, Butterworth-Heinemann Ltd., Oxford, 1992
21. G. Spanos, R.W. Fonda, R.A. Vandermeer, and A. Matuszeski, Microstructural Changes in HSLA-100 Steel Thermally Cycled to Simulate the Heat-Affected Zone during Welding, *Metall. Mater. Trans. A*, 1995, **26**, p 3277–3293
22. H.W. Paxton, Experimental Verification of the Twin System in Alpha-Iron, *Acta Metall.*, 1953, **1**, p 141–143
23. K. Poorhaydari, B.M. Patchett, and D.G. Ivey, Transformation Twins in the Weld HAZ of a Low-Carbon High-Strength Microalloyed Steel, *Mater. Sci. Eng. A*, 2006, **435**, p 371–382
24. S. Kou, Welding Metallurgy, Second Edition 2003, p 170–176
25. S.A. David, S.S. Babu, and J.M. Vitek, Welding: Solidification and Microstructure, *JOM*, 2003, **55**(6), p 14–20
26. A. Basak and S. Das, Epitaxy and Microstructure Evolution in Metal Additive Manufacturing, *Annu. Rev. Mater. Res.*, 2016, **46**(1), p 125–149
27. E. Hinchy, M.J. Pomeroy, and J. Michael, The Effect of Single Crystal and Welded Substrates on the Development of Braze Microstructures, *J. Alloys Compd.*, 2017, **690**, p 856–863
28. A. Keshavarzkermani, M. Sadowski, and L. Ladani, Direct Metal Laser Melting of Inconel 718: Process Impact on Grain Formation and Orientation, *J. Alloys Compd.*, 2018, **736**, p 297–305
29. Z. Lei and N. Lu, Epitaxy and New Stray Grain Formation Mechanism during Epitaxial Laser Melting Deposition of Inconel 718 on Directionally Solidified Nickel-Based Superalloys, *J. Manuf. Process.*, 2019, **42**, p 11–19
30. T.M. Pollock and W.H. Murphy, The Breakdown of Single-Crystal Solidification in High Refractory Nickel-Base Alloys, *Metall. Mater. Trans. A*, 1996, **27**(4), p 1081–1094
31. T.D. Anderson, J.N. DuPont, and T. DebRoy, Stray Grain Formation in Welds of Single Crystal Ni-Base Superalloy CMSX-4, *Metall. Mater. Trans. A*, 2010, **41**(1), p 181–193
32. M. Gaumann, S. Henry, F. Cleton, J.D. Wagniere, and W. Kurz, Epitaxial Laser Metal Forming: Analysis of Microstructure Formation, *Mater. Sci. Eng. A*, 1999, **271**(1), p 232–241
33. G. Palumbo, K.T. Aust, E.M. Lehockey, U. Erb, and P. Lin, On a More Restrictive Geometric Criterion for "Special" CSL Grain Boundaries, *Scr. Mater.*, 1998, **38**, p 1685–1690
34. K.J. Al-Fadhalah, Texture and Grain Boundary Character Distribution in a Thermomechanically Processed OFHC Copper, *J. Eng. Mater. Technol.*, 2012, **134**, p 011001–011009
35. G. Chen, Y. Zhang, D.K. Xu, Y.C. Lin, and X. Chen, Low Cycle Fatigue and Creepfatigue Interaction Behavior of Nickel-Base Superalloy GH4169 at Elevated Temperature of 650°C, *Mater. Sci. Eng. A*, 2016, **655**, p 175–182
36. K. Deepak, M. Sumantra, C.N. Athreya, D.I. Kim, and B. de Boer, Implication of Grain Boundary Engineering on High Temperature Hot Corrosion of Alloy 617, *Corros. Sci.*, 2016, **106**, p 293–297

37. B. Li and S. Tin, The Role of Deformation Temperature and Strain on Grain Boundary Engineering of Inconel 600, *Mater. Sci. Eng. A*, 2014, **603**, p 104–113
38. A. Rollett, F.J. Humphreys, and G.S. Rohrer, *Recrystallization and Related Annealing Phenomena*, Elsevier Science, Amsterdam, 2004